Optical resolution of oriented enantiomers via photodissociation: quantum model simulations for H_2POSD

Leticia González[a], Jörn Manz[a], Burkhard Schmidt[b], Mohamed F. Shibl[a]

[a] *Institut für Chemie und Biochemie-Physikalische und Theoretische Chemie, Freie Universität Berlin, Takustrasse 3, 14195 Berlin, Germany*

[b] *Institut für Mathematik II, Freie Universität Berlin, Arnimallee 2-6, 14195 Berlin, Germany*

Abstract

We demonstrate quantum mechanically how to resolve enantiomers from an oriented racemic mixture taking advantage of photodissociation. Our approach employs a femtosecond ultraviolet (UV) laser pulse with specific linear polarization achieving selective photodissociation of one enantiomer from a mixture of L and D enantiomers. As a result, the selected enantiomer is destroyed in the electronically excited state while the opposite enantiomer is left intact in the ground state. As an example we use H_2POSD which presents axial chirality. A UV pulse excites the lowest singlet excited state which has $n\sigma^*$ character and is, therefore, strongly repulsive along the P—S bond. The model simulations are performed using wavepackets which propagate on two dimensional potential energy surfaces, calculated along the chirality and dissociation reaction coordinates using CASSCF level of theory.

1. Introduction

Using tailored laser pulses femtosecond chemistry can nowadays control a large variety of elementary reactions—photodissociation[1], bond rearrangement,[2] or selective molecular excitation,[3] are just few examples.[4] Control of photoisomerization, however, is in an early experimental stage, and in particular, control of molecular chirality still remains challenging. On the theoretical side, it is encouraging that different methods are being proposed to predict preferential synthesis of a single enantiomer from a racemic mixture of two enantiomers by means of laser pulses. These methods include the work of Fujimura and coworkers on helical enantiomers,[5] as well as the method of "laser

distillation"[6] or "two-step enantio-selective switch"[7] proposed by Shapiro, Brumer and coworkers, with applications to 1,3-dimethylallene and S_2H_2. The so-called laser distillation method repeatedly makes use of three linearly polarized, perpendicular laser pulses to purify chiral substances in a randomly oriented sample,[6] whereas the two-step method employs only two—a pump and a dump—laser pulses.[7] Another distillation approach has been discussed by Bychkov et al. employing coherent entanglement of the rotational-torsional states of the molecules.[8] In passing we note, that such molecular states can be used to prepare coherent superpositions with the purpose of quantum information processing, as shown e.g. by Sola and coworkers, who used H_2POSH to encode a two-qubit.[9] Last but not least, we have suggested laser purification of a preoriented racemic sample, with applications to H_2POSH[10,11,12,13,14] and chiral olefins[15,16].

In this paper we extend a concept which has been introduced previously by our group, in order to encourage experiments on enantiomer purification from a racemate. As a prerequisite, it is assumed that the racemate is pre-oriented, e.g. in oriented environments, like surfaces or matrices, or e.g. by means of intense elliptically polarized laser fields, as suggested by Seideman and Stapelfeldt.[17] Essentially, a single linearly polarized laser pulse excites selectively the undesired enantiomer to a repulsive electronic excited state, this enantiomer dissociates, and in this way it is eliminated out of the racemic mixture. This approach was tested preliminarily for a single one-dimensional (1d) model of H_2POSD, using exclusively the chiral reaction coordinate, i.e. the OPDS torsional angle. The first excited state of H_2POSD shows $n\sigma^*$ character and exhibits, therefore, a dissociative surface which leads to an electrostatic repulsion between the fragments H_2PO and SD. In the present work, we include the decisive dissociation coordinate, demonstrating that optical resolution of enantiomers is indeed feasible. Our simulations show, however, that due to weak dipole couplings between the initial and the intermediate excited state the amount of population transferred—and therefore, the efficiency—is considerably reduced in comparison with our previous 1d model. Note that in the present case, we turn competing photodissociation to our advantage, that is, ultrafast dissociation is used to eliminate the undesired enantiomers. In contrast, if one aims at interconverting the undesired enantiomer into the useful one,

we have also shown that a sequential pump-dump scenario may be used to suppress the undesired photodissociation.[18]

The paper is organized as follows: the model system, relevant quantum chemical calculations and Hamiltonian are presented in Section 2. Section 3 discusses the numerical results achieved for the separation of H_2POSD enantiomers, and finally, Section 4 summarizes our results.

2. Theory

2.1 The H_2POSD molecule and electronic structure calculations.

The proposed mechanism shall be demonstrated for the deuterated phosphinothioic acid, H_2POSD which presents (transient) axial chirality. Fig. 1a shows the molecule in the molecular frame (x,y,z) with the atom P at the origin and the OPS fragment in the x/z plane; the P—S bond is along the z-axis and it is denoted by r. The chiral coordinate is the OPSD torsional angle ϕ around the z-axis. For the quantum dynamics simulation, we consider the system in the laboratory frame (X,Y,Z) with orientation as shown in Fig. 1b. Here r' is the distance between the center of mass (c.o.m) of OPH_2 and the c.o.m. of SD, and ϕ' is the relative rotation of SD with respect to OPH_2, i.e. the angle between the planes OPS and DSP.

Upon ultraviolet (UV) irradiation, the molecule undergoes P—S bond fragmentation. The relevant molecule-fixed and laboratory fixed coordinates are thus r and ϕ or r' and ϕ', respectively. Extending our preliminary 1d calculations, the electronic ground, $V_0(r,\phi)$, and first excited singlet state $V_1(r,\phi)$ potential energy surfaces (PES) are calculated varying the distance r equidistantly from 3.1 to 11.4 bohrs and the angle ϕ from 0 to π radians, obtaining 299 ab initio points. Taking into account symmetry, we rely on a 2d PES composed of a total number of 575 ab initio grid points. The remaining degrees of freedom have been kept frozen at the equilibrium geometry. Treating electronically excited states and dissociative problems require multiconfigurational methods; accordingly, our PESs are calculated using the complete

active space self-consistent field (CASSCF), as implemented in the MOLCAS4.3 quantum chemical software package.[19] Because the ground and excited states are degenerate in the asymptotic region, both roots are calculated with state averaging (SA) of equal weights. The active space comprises 14 electrons correlated in 12 active orbitals, including the lone pairs of the oxygen and sulfur atoms, the bonding/antibonding σ,σ^* pairs of the P-S and P=O bonds, and Rydberg orbitals. With this active space, the lowest singlet state is mainly a HOMO-LUMO transition, characterized by an excitation of an electron from the lone pair of the S atom to an antibonding P—S orbital (n_S-$\sigma^*_{P\text{-}S}$ excitation). The SA-2-CASSCF calculations were made with the ANO-L basis set of the size (17s12p5d) primitives contracted to [4s3p2d] for the P- and S-atoms, (14s9p4d) contracted to [4s3p2d] for the O-atom, and (8s4p) contracted to [3s2p] for the H-atoms, summing up to a total number of 114 contracted basis functions. The electronic transition dipole moment surface has been obtained at the same level of theory as the PES.

2.2. Hamiltonian

The laser driven time evolution of the molecular system in the two PES of interest, V_0 and V_1, is described by the Liouville equation

$$i\hbar \frac{\partial \rho(t)}{\partial t} = \left[\hat{H}(t), \rho(t)\right], \tag{1}$$

where the time-dependent density matrix is given by

$$\rho(t) = \begin{pmatrix} \rho_{00}(t) & \rho_{01}(t) \\ \rho_{10}(t) & \rho_{11}(t) \end{pmatrix}, \tag{2}$$

with densities $\rho_{ij} = \left|\Psi^i(t)\right\rangle\left\langle\Psi^j(t)\right|$, assuming non-dissipative environment. The indices *i* and *j* represent the electronic states 0 and 1. The Hamiltonian $\hat{H}(t)$ is written as

$$\hat{H}(t) = \begin{pmatrix} \hat{H}_{00} & \hat{H}_{01} \\ \hat{H}_{10} & \hat{H}_{11} \end{pmatrix} = \begin{pmatrix} \hat{T}_n + V_0 & -\vec{\mu}_{01}\vec{\varepsilon}(t) \\ -\vec{\mu}_{10}\vec{\varepsilon}(t) & \hat{T}_n + V_1 \end{pmatrix}. \tag{3}$$

Neglecting non-adiabatic couplings, the nuclear kinetic operator $\hat{T}_{\mathrm{n}}$ and the electronic potentials V_{i} compose the molecular Hamiltonian, while the terms - $\vec{\mu}_{ij}\vec{\varepsilon}(t)$ describe the interaction with laser radiation in the semiclassical dipole approximation. The transition dipole moment vector between the *i* and *j* states is given by $\vec{\mu}_{ij}=\vec{\mu}_{ji}$, and $\vec{\varepsilon}(t)$ is the electric field vector specified as

$$\vec{\varepsilon}(t)=\vec{e}\ \varepsilon^{0}\cos(\omega t+\eta)s(t) \tag{4}$$

where $\vec{e}$ is the polarization vector, ε^{0} is the field amplitude, ω is the carrier frequency, η is the phase, and *s(t)* is the shape function $s(t)=\sin^{2}(\pi\ t/t_{p})$ for $0 \le t \le t_{\mathrm{p}}$, with pulse duration $t_{p.}$ Since the subsequent application deals with UV excitations, the permanent dipole couplings - $\vec{\mu}_{ii}\vec{\varepsilon}(t)$ are negligible, and therefore, ignored.

At t = 0 the initial mixture is given by

$$\rho(t=0)=\begin{pmatrix}\rho_{00}(t=0) & 0\\ 0 & 0\end{pmatrix} \tag{5}$$

where

$$\rho_{00}(t=0)=\rho_{rac}(T) \tag{6}$$

represents a racemate of L and D enantiomers at temperature T (from now denoted as L and R for simplicity). Considering the limit of low T, the initial racemic mixture can be written as an incoherent superposition of the lowest doublet of eigenstates in the electronic ground state:

$$\rho_{rac}(T\to 0)\approx\frac{1}{2}\left|\psi^{0}_{00+}\right\rangle\left\langle\psi^{0}_{00+}\right|+\frac{1}{2}\left|\psi^{0}_{00-}\right\rangle\left\langle\psi^{0}_{00-}\right|=\frac{1}{2}\left|\Psi^{0}_{00L}\right\rangle\left\langle\Psi^{0}_{00L}\right|+\frac{1}{2}\left|\Psi^{0}_{00R}\right\rangle\left\langle\Psi^{0}_{00R}\right| \tag{7}$$

The $\left|\psi^{0}_{00+}\right\rangle$ and $\left|\psi^{0}_{00-}\right\rangle$ states are vibrational eigenfunctions of the electronic ground state $\left|\Psi^{0}\right\rangle$ obtained as solutions of the time-independent Schrödinger equation,

$\left(\hat{T}_n + V_0\right)\left|\psi^0_{\nu\pm}\right\rangle = E^0_{\nu\pm}\left|\psi^0_{\nu\pm}\right\rangle$, with vibrational quantum numbers $\nu = (\nu_\tau, \nu_s)$ for the torsion τ and the P—S stretch *s*, and with symmetry + or – along the torsional motion. The localized wavefunctions $\left|\Psi^0_{00L}\right\rangle$ and $\left|\Psi^0_{00R}\right\rangle$ correspond to L or R-enantiomers in the lowest doublet of states, and, in general, they are constructed as coherent superpositions of the torsional eigenstates of different parity:

$$\begin{aligned}\Psi^0_{\nu L} &= \frac{1}{\sqrt{2}}\left(\left|\psi^0_{\nu+}\right\rangle + \left|\psi^0_{\nu-}\right\rangle\right)\\ \Psi^0_{\nu R} &= \frac{1}{\sqrt{2}}\left(\left|\psi^0_{\nu+}\right\rangle - \left|\psi^0_{\nu-}\right\rangle\right)\end{aligned} \tag{8}$$

Because we do not include any dissipation term in Eq. (1), the solution of the Liouville-equation is equivalent to the independent solutions of the time-dependent Schrödinger equation for the L and R densities,

$$i\hbar\frac{d}{dt}\begin{pmatrix}\Psi^0_{00L}(t)\\ \Psi^1_{00L}(t)\end{pmatrix} = \begin{pmatrix}\hat{T}_n + V_0 & -\vec{\mu}_{01}\vec{\varepsilon}(t)\\ -\vec{\mu}_{10}\vec{\varepsilon}(t) & \hat{T}_n + V_1\end{pmatrix}\begin{pmatrix}\Psi^0_{00L}(t)\\ \Psi^1_{00L}(t)\end{pmatrix} \tag{9a}$$

$$i\hbar\frac{d}{dt}\begin{pmatrix}\Psi^0_{00R}(t)\\ \Psi^1_{00R}(t)\end{pmatrix} = \begin{pmatrix}\hat{T}_n + V_0 & -\vec{\mu}_{01}\vec{\varepsilon}(t)\\ -\vec{\mu}_{10}\vec{\varepsilon}(t) & \hat{T}_n + V_1\end{pmatrix}\begin{pmatrix}\Psi^0_{00R}(t)\\ \Psi^1_{00R}(t)\end{pmatrix}. \tag{9b}$$

Instead of the internal bond-angle coordinates *r* and ϕ (cf. Fig. 1a), we will employ the laboratory fixed *r*′ and ϕ′ coordinates (cf. Fig. 1b) to solve Eqs. (9a-b). The corresponding kinetic energy operator $\hat{T}'_n$ is given as (see Ref. 20):

$$\hat{T}'_n = \frac{-\hbar^2}{2I_{SD,OPH_2}}\frac{d^2}{d\phi'^2} + \frac{-\hbar^2}{2m_r}\frac{d^2}{dr'^2} \tag{10}$$

where I_{SD,OPH_2} is the reduced moment of inertia,

$$I_{SD,OPH_2} = \frac{I_{SD}\,I_{OPH_2}}{I_{SD} + I_{OPH_2}}\,, \tag{11}$$

and m_r is the reduced mass of the SD and OPH_2 fragments. The corresponding potential energy surfaces V_i and transition dipole surfaces $\vec{\mu}'_{01}$ are then calculated from the original V'_i and $\vec{\mu}_{01}$, as described in Appendix A. In order to solve Eqs. (9a-b), the split-operator method,[21] implemented in the program package Wavepacket,[22] has been used with a time step of 0.05 fs.

3. Results and discussion

3.1. Potential energy surfaces, transition dipole surfaces and eigenfunctions

The ground V'_0 and singlet excited V'_1 PES of H_2POSD calculated at SA-2-CASSCF(14,12) level of theory as a function of r' and ϕ' are shown in Fig. 2. The PES V'_0 in the electronic ground state S_0 has two minima corresponding to L and R enantiomers. The barrier height is about 400 cm^{-1}. In contrast, the singlet excited state S_1 surface is repulsive along the P-S bond coordinate at the employed level of theory. The Franck-Condon vertical excitation energy at the (L) or (R) minima energy configurations is 5.81 eV. The repulsive character of the PES V'_1 along the P—S bond stems from the main configuration (n_S-$\sigma^*_{P\text{-}S}$) contributing to the first excited singlet state, in which an electron is promoted to an antibonding orbital. The X′,Y′ and Z′-transformed components of the transition dipole surfaces $\vec{\mu}'_{01}(r',\phi')$ are shown in Fig. 3. Accordingly, the μ'_{10X} and μ'_{10Z} surfaces are antisymmetric with respect to ϕ', while μ'_{10Y} is symmetric.

The torsional eigenstates $\left|\psi^0_{\nu\pm}\right\rangle$ of the electronic ground state $V'_0(r',\phi')$ are calculated using the Fourier Grid Hamiltonian technique[23] with a total of 8192= 256 x 32 splined grid points along the r' and ϕ' dimensions, respectively. The energy splitting, ΔE^0_ν, of the first three doublets is calculated as 0.02, 0.64, and 8.69 cm^{-1}, corresponding to L—R—L tunneling times, of 1.8 ns, 51.6 ps, and 3.8 ps, respectively.

3.2. Separation of H_2POSD enantiomers

In order to design a laser pulse which selects a single enantiomer out of an oriented racemic mixture, the direction of the polarization vector of the laser field has to be chosen conveniently. Excitation of a selected enantiomer will be suppressed if the electric field is perpendicular to the corresponding dominant transition dipole matrix element. In contrast, the interaction for the opposite enantiomer can be maximized if these two vectors are parallel. For instance, to excite the R enantiomer but not the L one to some final vibronic eigenstate $\left|\Psi_f\right\rangle$, $\vec{\mu}'$ and $\vec{\varepsilon}(t)$ should satisfy:

$$\begin{aligned}\left\langle\Psi_f\left|\vec{\mu}'\right|\Psi^0_{00L}\right\rangle\cdot\vec{\varepsilon}(t)\neq 0\\ \left\langle\Psi_f\left|\vec{\mu}'\right|\Psi^0_{00R}\right\rangle\cdot\vec{\varepsilon}(t)= 0\end{aligned} \qquad (12)$$

where $\left|\Psi^0_{00R}\right\rangle$ and $\left|\Psi^0_{00L}\right\rangle$ represent the initial R and L enantiomers, i.e. they are the localized functions in the R and L minima of the electronic ground state PES V_0' as defined in Eq. (8), respectively. In the present molecular system, however, the repulsive excited state potential V_1' does not support any bound states $\left|\Psi_f\right\rangle$. As a consequence, the rule given in Eq. (12) cannot be applied. In the following, we shall sketch how to proceed in such a case.

Let us consider a scenario where we start from one of the enantiomers, e.g. the R-one, i.e.,

$$\begin{pmatrix}\Psi^0(t=0)\\ \Psi^1(t=0)\end{pmatrix}=\begin{pmatrix}\Psi^0_{00R}\\ 0\end{pmatrix}. \qquad (13)$$

Using low laser intensities such that the population in V_1' remains small in comparison with the one in V_0', according to Eq. (9b) the change $\Delta\Psi^1_{00R}=\Psi^1_{00R}(t+\Delta t)-\Psi^1_{00R}(t)$ after a small time step Δt is approximately given by,

$$\Delta\Psi^1_{00R}\approx-\frac{\Delta t}{i\hbar}\vec{\mu}_{10}\vec{\varepsilon}(t)\Psi^0_{00R}(t=0)+\frac{\Delta t}{i\hbar}(\hat{T}_n+V_1')\Psi^1_{00R}(t)$$

$$= \Delta\Psi^1_{00R,c} + \Delta\Psi^1_{00R,e} \tag{14}$$

The first term of the r.h.s. represents the creation (c) of the wave packet in the excited state, while the second one accounts for its free evolution (e). Control can be exerted at the time the wave packet is created, and thus, we call this first term $\Delta\Psi^1_{00R,c}$, whereas the evolution term is compactly written as $\Delta\Psi^1_{00R,e}$. Using two components of the electric field which couple to the symmetric (μ'_Y) and antisymmetric (μ'_Z) components of $\vec{\mu}'$, the control term of Eq. (14) can be expanded as,

$$\Delta\Psi^1_{00R,c} = -\frac{\Delta t}{i\hbar}(\mu'_{10Y}\varepsilon_Y + \mu'_{10Z}\varepsilon_Z)\Psi^0_{00R}(t=0). \tag{15}$$

Similarly,

$$\Delta\Psi^1_{00L,c} = -\frac{\Delta t}{i\hbar}(\mu'_{10Y}\varepsilon_Y + \mu'_{10Z}\varepsilon_Z)\Psi^0_{00L}(t=0). \tag{16}$$

Then, the ratio between the electric field components ε_Y and ε_Z can be chosen such that the transition dipole interactions $(\mu'_{10Y}\varepsilon_Y + \mu'_{10Z}\varepsilon_Z)$ for example, minimizes the increments $\left\langle \Delta\Psi^1_{00L,c} \middle| \Delta\Psi^1_{00L,c} \right\rangle$, but constructively enhances $\left\langle \Delta\Psi^1_{00R,c} \middle| \Delta\Psi^1_{00R,c} \right\rangle$. This is illustrated in Fig. 4. Specifically, Figs. 4a and 4b show the initial localized wavefunctions $\Psi^0_{00L}(t=0)$ and $\Psi^0_{00R}(t=0)$, respectively (cf. Eq. 8), Figs. 4c and 4d show the products $\Psi^0_{00L}(t)\ \mu'_Z\varepsilon_Z$ and $\Psi^0_{00R}(t)\ \mu'_Z\varepsilon_Z$, and Figs. 4e and 4f show the analogous products $\Psi^0_{00L}(t)\ \mu'_Y\varepsilon_Y$ and $\Psi^0_{00L}(t)\ \mu'_Y\varepsilon_Y$, respectively. Note the different signs of the lobes of the wave function due to the opposite symmetries of μ_Y and μ_Z. Finally, Figs. 4g and 4h show the resulting wave functions for $\Psi^0_{00L}(\mu'_Y\varepsilon_Y + \mu'_Z\varepsilon_Z)$ and $\Psi^0_{00R}(\mu'_Y\varepsilon_Y + \mu'_Z\varepsilon_Z)$. The laser parameters used correspond to a linearly polarized laser field with components ε_Z = 2 GV/m and ε_Y = 1.75 ε_Z. Apparently, the increment $\Delta\Psi^1_{00L,c}$ is almost negligible while $\Delta\Psi^1_{00R,c}$ has been enhanced constructively. Analogous polarizations could be used to minimize $\Delta\Psi^1_{00R,c}$ —in this case a field of

ε_Y = - 1.75 ε_Z would be needed. Therefore, control of the polarization of the electric field allows exciting just one enantiomer, whereas the other enantiomer remains in its ground state ($\Delta\Psi^1_{00L,c}$ or $\Delta\Psi^1_{00R,c}$ =0).

After having considered the case of δ-pulse, we proceed to apply the strategy described above to excite one enantiomer from a racemic mixture using a real laser pulse. As an example, the resulting selective photoexcitation of the R enantiomer from a racemate is demonstrated in Fig. 5, showing snapshots of the L and R wave packet in the electronic ground state S_0 at t=0 fs, and in the electronic excited state S_1 after 95 fs. The laser parameters obtained in previous instructive example serve as a reference for the case considered now. We employ the same laser components, ε_Z = 2 GV/m and ε_Y = 3.5 GV/m, and the remaining optimized laser parametes are ω=5.884 eV, t_p=100 fs and η=0°. Since the P—S bond breaking occurs on a fs scale, very short pulses have been used. The polarization angle resulting from the ε_Y and ε_Z components is 29.7°. Due to the weak transition dipole couplings the population excited to the singlet state is about 5%, in accord with the assumption underlying Eq. (14). However, the R enantiomer is successfully excited to the S_1 singlet state by a factor of ca. 20 more efficiently than the L enantiomer (cf. Fig. 5a) demonstrating the selectivity of the applied laser pulses. The singlet state is strongly repulsive, and therefore, after 95 fs the R enantiomer has completely dissociated. Notice that the photodissociation path followed by the wave packet is tilted due to the achiral nature of the S_1 PES, which possesses a single minimum along the torsional reaction coordinate; as a result the dissociating fragments rotate with respect of each other. By virtue of this ultrafast photodissociation process we have therefore optically resolved the racemic mixture, eliminating the R-enantiomer by factor 20 against the L-enantiomer. Similar to the distillation approaches suggested in Ref. 6, in an iterative manner it should be possible to resolve the L-enantiomer by 100% from a racemic sample.

4. Conclusion

Two-dimensional quantum dynamical simulations on the model system H_2POSD have been employed to demonstrate that optical resolution of oriented enantiomers taking

advantage of selective photodissociation is feasible. The underlying concept is to use a linearly polarized laser field with a polarization direction which makes the transition dipole interaction with one of the enantiomer vanishing, while constructively enhancing the other enantiomer. In this way, only one enantiomer is excited to some intermediate state, while the other remains mostly unexcited in the electronic ground state. If the intermediate state is a repulsive electronic excited state the excited enantiomer will dissociate, while the counterpart does not. Repeated applications of the laser pulses will accumulate the target enantiomer while dissociate the other one.

Acknowledgement:

Generous financial support for this project by the Deutsche Forschungsgemeinschaft (Project Ma 515/18-3) and Fonds der Chemischen Industrie are gratefully acknowledged.

Figure captions

Figure 1. Molecular orientation of H_2POSD, with dissociative and torsional coordinates. (a) shows the molecule fixed coordinates r and ϕ, which describe the P—S distance and the torsional angle OPSD, respectively. (b) shows the laboratory coordinates r' and ϕ', which describe the distance between the centers of masses of the SD and H_2PO fragments, and the corresponding torsional motion between them, respectively.

Figure 2. Contour plots of the potential energy surfaces of H_2POSD calculated at SA-2-CASSCF(14,12) level of theory as a function of the torsion angle ϕ' (in radians) and the distance r' (in bohrs) between the fragments H_2PO and SD. Panels (a) and (b) are for the electronic ground state V_0' (S_0) and the first electronic singlet excited state V_1' (S_1) respectively. The contour lines are drawn from 0.01 eV until 0.2 eV at regular intervals of 0.01 for V_0', and from 3 eV until 6.2 eV at regular intervals of 0.1 for V_1'; the zero energy is located at the minimum of the S_0 surface.

Figure 3. Contours plots of the X,Y and Z components of the transition dipole moment of H_2POSD, as a function of the torsion angle ϕ' (in radians) and the distance r' (in bohrs) between the fragments H_2PO and SD. The lines are drawn from -0.08 to 0.08 in intervals of 0.01 for X-component, from -0.03 to 0.03 in intervals of 0.005 for Y-component and from -0.05 to 0.05 in intervals of 0.01 for Z-component (in ea_0). Solid are positive values, dashed are negative values.

Figure 4. Constructive and destructive interferences of the $\Psi_{00L}^{0}(t)$ and $\Psi_{00R}^{0}(t)$ wavefunctions with dipole interactions. The contours in (a) and (b) show the localized $\Psi_{00L}^{0}(t=0)$ and $\Psi_{00R}^{0}(t=0)$ initial wave functions, respectively. The contours in (c-h) show the corresponding wavefunctions after multiplication with appropriate dipole interactions (see label). ε_Z =2 GV/m and ε_Y = 3.5 GV/m.

Figure 5. Photofragmentation induced in the R-enantiomer, while the L counterpart stays in the electronic ground state S_0. (a) Probability density in the S_1 at t=95 fs. (b) Probability density of the racemic mixture at initial time in the electronic ground state S_0.

Appendix A. Coordinate transformation

In this Appendix we derive an expression that relates the original molecule fixed coordinates *r* and ϕ to new laboratory coordinates *r'* and ϕ'. We recall that *r* and ϕ describe the P—S bond length and the dihedral angle defined by the atoms OPSD, corresponding to the torsional angle of the SD versus OPH_2 fragments around the S-P bond, respectively, whereas *r'* and ϕ' are defined as the distance between the c.o.m.'s of the SD and OPH_2 fragments and the torsion of SD versus OPH_2 fragments around the line connecting the c.o.m.'s of the SD and OPH_2 fragments, see Figure 1. We assume that the line *(r')* is oriented along the laboratory fixed Z axis, and the atoms O and P remain in the X/Z plane.

Let the c.o.m of OPH_2 fragment be the origin of the laboratory fixed coordinates, $\vec{r}'_{c.o.m,OPH_2} = \vec{0}$. Then (in bohrs)

$$\vec{r}'_P = \begin{bmatrix} 0.74 \\ 0.00 \\ 0.45 \end{bmatrix}, \tag{A1}$$

$$\vec{r}'_O = \begin{bmatrix} -1.72 \\ 0.00 \\ -0.87 \end{bmatrix}, \tag{A2}$$

$$\vec{r}'_{OP} = \begin{bmatrix} 2.46 \\ 0.00 \\ 1.32 \end{bmatrix}. \tag{A3}$$

and

$$\vec{r}' = \vec{r}'_{c.o.m,SD} - \vec{r}'_{c.o.m,OPH_2} = \vec{r}'_{c.o.m,SD} = c_D \vec{r}'_D + c_S \vec{r}'_S \tag{A4}$$

with $c_D = \dfrac{m_D}{m_D + m_S}$ and $c_S = \dfrac{m_S}{m_D + m_S}$.

Also,

$$\vec{r}'_{SD} = \vec{r}'_D - \vec{r}'_S \tag{A5}$$

From the matrix representation of Eqs. (A4) and (A5)

$$\begin{pmatrix} \vec{r}' \\ \vec{r}'_{SD} \end{pmatrix} = \begin{pmatrix} c_D & c_S \\ 1 & -1 \end{pmatrix} \begin{pmatrix} \vec{r}'_D \\ \vec{r}'_S \end{pmatrix}, \tag{A6}$$

we obtain

$$\begin{pmatrix} \vec{r}'_D \\ \vec{r}'_S \end{pmatrix} = \begin{pmatrix} 1 & c_S \\ 1 & -c_D \end{pmatrix} \begin{pmatrix} \vec{r}' \\ \vec{r}'_{SD} \end{pmatrix} = \begin{pmatrix} \begin{pmatrix} 0 \\ 0 \\ r' \end{pmatrix} + c_s r'_{SD} \begin{pmatrix} \sin\theta' \cos\phi' \\ \sin\theta' \sin\phi' \\ \cos\theta' \end{pmatrix} \\ \begin{pmatrix} 0 \\ 0 \\ r' \end{pmatrix} - c_D r'_{SD} \begin{pmatrix} \sin\theta' \cos\phi' \\ \sin\theta' \sin\phi' \\ \cos\theta' \end{pmatrix} \end{pmatrix} \tag{A7}$$

where θ' is the polar angle defined by the Z axis and the $\vec{r}'_{SD}$, fixed to 0.52 π. The length, r'_{SD}, is fixed to 2.53 bohrs. Eqns. (A1) and (A7) allow to calculate

$$\vec{r}'_{PS} = \vec{r}'_S - \vec{r}'_P \tag{A8}$$

and finally to express *r* in terms of r' and ϕ',

$$r = r_{SP} = \left|\vec{r}'_S - \vec{r}'_P\right| = \sqrt{(r'_{S_X} - r'_{P_X})^2 + (r'_{S_Y} - r'_{P_Y})^2 + (r'_{S_Z} - r'_{P_Z})^2}\,. \tag{A9}$$

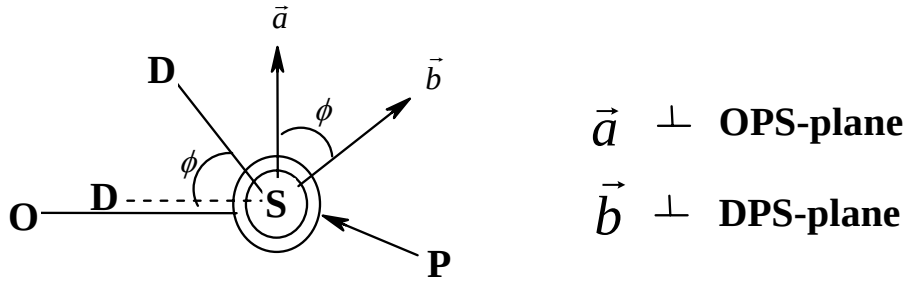

Scheme I

Next, we derive an expression for ϕ in terms of r' and ϕ'. For this purpose, we note from Scheme I that ϕ is the angle between the OPS- and DPS-planes, i.e. ϕ is also the angle between two vectors $\vec{a}$ and $\vec{b}$ perpendicular to these planes,

$$\phi = \arccos\left(\frac{\vec{a}' \cdot \vec{b}'}{\left|\vec{a}'\right| \cdot \left|\vec{b}'\right|}\right) \tag{A10}$$

Using Eqs. (A3), (A6), and (A8) we obtain:

$$\vec{a}' = \frac{\vec{r}'_{OP} \times \vec{r}'_{PS}}{\left|\vec{r}'_{OP} \times \vec{r}'_{PS}\right|} \tag{A11}$$

and

$$\vec{b}' = \frac{\vec{r}'_{PS} \times \vec{r}'_{SD}}{\left|\vec{r}'_{PS} \times \vec{r}'_{SD}\right|} . \tag{A12}$$

Eqs. (A4), (A7) and (A10)-(A12) then allow to calculate ϕ in terms of r' and ϕ'.

This transformation from r' and ϕ' to corresponding values of r and ϕ' yields e.g. the potential energy surface in the new coordinates:

$$V'(r', \phi') = V(r(r', \phi'), \phi(r', \phi')) , \tag{A13}$$

which is written in a grid representation as follows:

$$V'(r'_i, \phi'_j) = V(r\{r'_i, \phi'_j\}, \phi\{r'_i, \phi'_j\}) . \tag{A14}$$

References

[1] A. Assion, T. Baumert, M. Bergt, T. Brixner, B. Kiefer, V. Seyfried, M. Strehle and G. Gerber, *Science*, 1998**,** **282**, 919; C. Daniel, J. Full, L. González, C. Lupulescu, J. Manz, A. Merli, S. Vajda and L. Wöste, *Science*, 2003, **299**, 536.

[2] R. J. Levis, G. M. Menkir, and H. Rabitz, *Science*, 2001, **292**, 709.

[3] T. Brixner, N. H. Damrauer, P. Niklaus and G. Gerber *Nature*, 2001, **414**, 57.

[4] For recent reviews, S. A. Rice and M. Zhao, *Optical Control of Molecular Dynamics*, Wiley-Interscience, 2000; M. Shapiro and P. Brumer, *Principles of the Quantum Control of Molecular Processes* **,** Wiley-Interscience, 2003.

[5] H. Umeda, M. Takagi, S. Yamada, S. Koseki and Y. Fujimura, *J. Am. Chem. Soc.*, 2002, **124**, 9265.

[6] M. Shapiro, E. Frishman and P. Brumer, *Phys. Rev. Lett.,* 2000, **84**, 1669; E. Frishman, M. Shapiro, D. Gerbasi and P. Brumer, *J. Chem. Phys.*, 2003, **119**, 7237.

[7] P. Král, I. Thanopulos, M. Shapiro and D. Cohen, *Phys. Rev. Lett.*, 2003, **90**, 033001; D. Gerbasi, P. Brumer, I. Thanopulos, P. Král and M. Shapiro, *J. Chem. Phys.*, 2004, **120**, 11557; I. Thanopulos, E. Paspalakis and Y. Kis, *Chem. Phys. Lett.*, 2004, **390**, 228.

[8] S. S. Bychkov, B. A. Grishanin, V. N. Zadkov and H. Takahashi, *J. Raman Spectrosc.,* 2002, **33**, 962.

[9] I. R. Sola, V. Malinovsky and J. Santamaria, *J. Chem. Phys.*, 2004, **120**, 10955.

[10] Y. Fujimura, L. González, K. Hoki. D. Kröner, J. Manz and Y. Ohtsuki, *Angew. Chem. Int. Ed.,* 2000, **39**, 4586; Y. Fujimura, L. González, K. Hoki, J. Manz, Y. Ohtsuki and H. Umeda, *Advances in Multiphoton Processes and Spectroscopy* (World Scientific, Singapore, 2001, Vol. 14, p. 30; K. Hoki, Y. Ohtsuki and Y. Fujimura, *J. Chem. Phys.,* 2001, **114**, 1575.

[11] L. González, D. Kröner and I. R. Solá, *J. Chem. Phys.,* 2001, **115**, 2519.

[12] K. Hoki, D. Kröner and J. Manz, *Chem. Phys.*, 2001, **267**, 59.

[13] K. Hoki, L. González and Y. Fujimura, *J. Chem. Phys.,* 2002, **116**, 2433; K. Hoki, L. González and Y. Fujimura, *J. Chem. Phys.*, 2002, **116**, 8799

[14] Y. Ohta, K. Hoki and Y. Fujimura, *J. Chem. Phys.*, 2002, **116**, 7509.

[15] D. Kröner, M. F. Shibl and L. González, *Chem. Phys. Lett.*, 2003, **372**, 242.

[16] D. Kröner and L. González, *Phys. Chem. Chem. Phys.*, 2003, **5**, 3933 ; D. Kröner and L. González, *Chem. Phys.*, 2004, **298**, 55.

[17] J. J. Larsen, K. Hald, N. Bjerre, H. Stapelfeldt and T. Seideman, *Phys. Rev. Lett.*, 2000, **85**, 2470; H. Stapelfeldt and T. Seideman, *Rev. Mod. Phys.*, 2003, **75**, 543

[18] K. Hoki, L. González, M. F. Shibl and Y. Fujimura, *J. Phys. Chem. A*, 2004, **108**, 6455.

[19] K. Andersson, M. R. Blomberg, M. P. Fülscher, G. Karlström, R. Lindh, P.-Å. Malmqvist, P. Neogrady, J. Olsen, B. O. Roos, A. J. Sadlej, M. Schütz, L. Seijo, L. Serrano-Andres, P. E. M. Siegbahn and B.-O. Widmark, MOLCAS 4.1, Lund University, Sweeden, 1998.

[20] J. Manz, *Molec. Phys.*, 1971, **21**, 641.

[21] M. D. Feit and J. A. Fleck Jr., *J. Chem. Phys.*, 1983, **78**, 301.

[22] B. Schmidt et al., Wavepacket 3.0: a Program Package For Wavepacket Propagation and Time-Dependent Spectroscopy, Free University Berlin, Germany, 2003.

[23] C. C. Marston and G. G. Balint-Kurti, *J. Chem. Phys.*, 1989**, 91**, 3571.

Figure 1

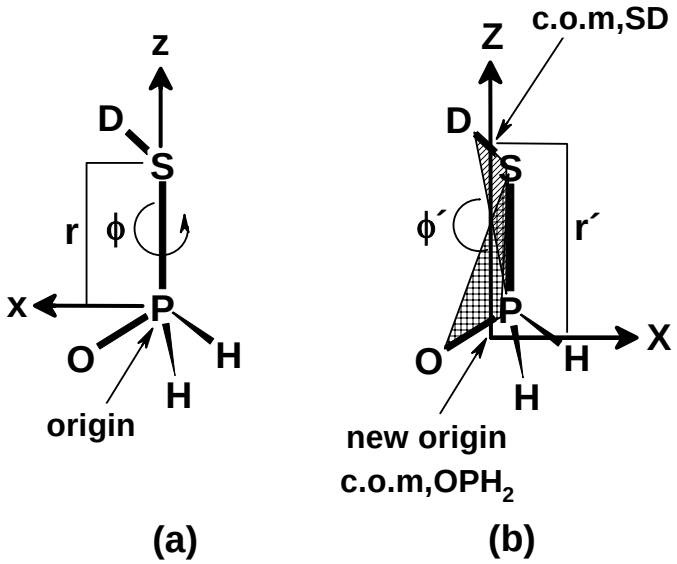

Figure 2

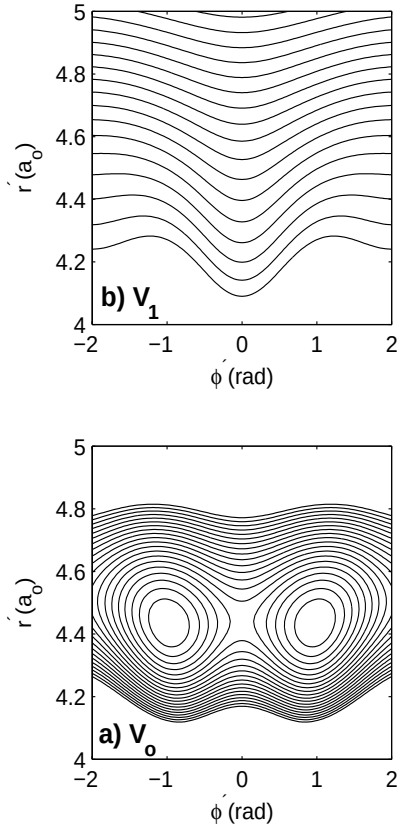
5
4.8
4.6
4.4
4.2
4
r´(a_o)
b) V_1
−2
−1
0
1
2
φ´(rad)
5
4.8
4.6
4.4
4.2
4
r´(a_o)
a) V_o
−2
−1
0
1
2
φ´(rad)

Figure 3

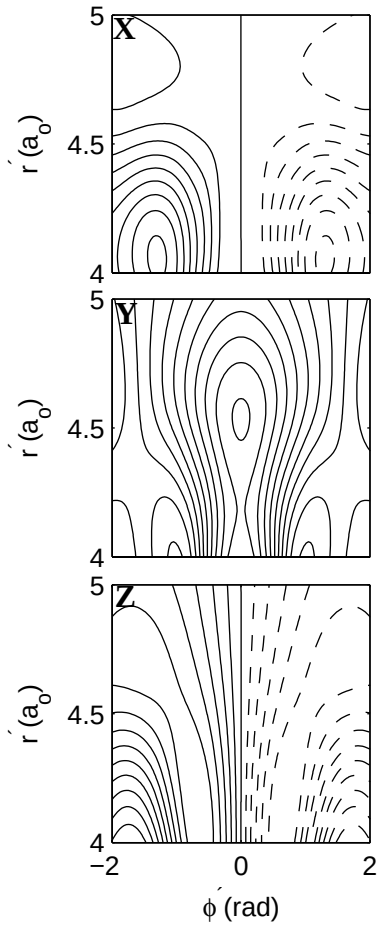

Figure 4

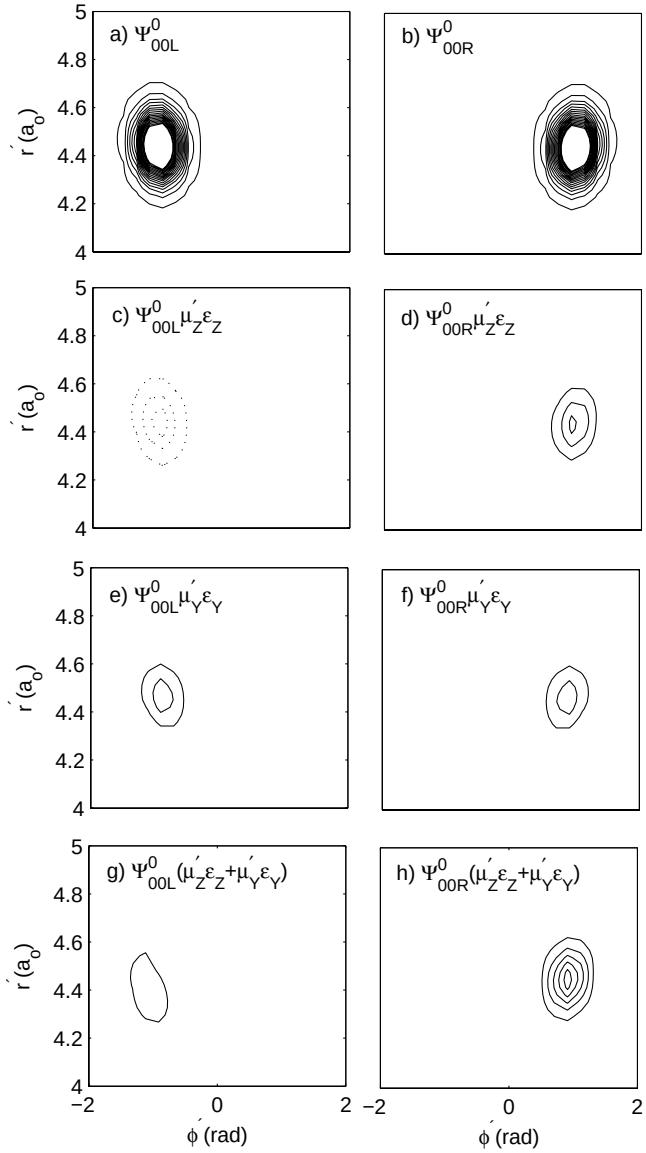
a) Ψ^0_{00L}
b) Ψ^0_{00R}
c) $\Psi^0_{00L}\mu'_Z\varepsilon_Z$
d) $\Psi^0_{00R}\mu'_Z\varepsilon_Z$
e) $\Psi^0_{00L}\mu'_Y\varepsilon_Y$
f) $\Psi^0_{00R}\mu'_Y\varepsilon_Y$
g) $\Psi^0_{00L}(\mu'_Z\varepsilon_Z+\mu'_Y\varepsilon_Y)$
h) $\Psi^0_{00R}(\mu'_Z\varepsilon_Z+\mu'_Y\varepsilon_Y)$
r´ (a_0)
5
4.8
4.6
4.4
4.2
4
−2
0
2
φ´ (rad)

Figure 5.